Int. J. Heat Mass Transfer. Vol. 35, No. 8, pp. 1987–2004, 1992
Printed in Great Britain

0017–9310/92 $5.00 + 0.00

Dropwise evaporation : thermal analysis of multidrop systems

KEK-KIONG TIO
Department of Applied Mechanics and Engineering Sciences, University of California, San Diego, La Jolla, CA 92093-0411, U.S.A.

and

SATWINDAR SINGH SADHAL
Department of Mechanical Engineering, University of Southern California, Los Angeles, CA 90089-1453, U.S.A.

(*Received* 21 *August* 1990 *and in final form* 26 *July* 1991)

Abstract—This paper investigates the heat transfer from a heated solid surface to droplets evaporating in the low superheat regime, where the droplets stick onto the surface without bubble nucleation. The model consists of a regular array of identical droplets interacting thermally through the solid. Analytical expressions for the Nusselt number involving a power series of $\kappa^{1/2}$, where κ is the fraction of the solid surface wetted by the droplets, are derived. It is found that droplet interactions cannot, in general, be ignored. Furthermore, the strength of these interactions is a function of droplet contact angle, solid conductivity, and droplet concentration.

1. INTRODUCTION

THE EVAPORATION of droplets at a heated solid surface can be classified into three categories, depending on the temperature of the solid surface in excess of the droplet saturation temperature. Specifically, these are low superheat, intermediate superheat, and high superheat. In the region of low superheat evaporation, the droplets maintain total contact with the solid surface over their entire lifetime. While the convective effect may be significant in some cases, many investigators [1–5] believe that conduction is the dominant heat transfer mechanism inside the droplets. Furthermore, it appears that no analytical study incorporating convective heat transfer exists in the literature, although fluid motion within the droplets has been observed experimentally [6, 7]. For sufficiently low surface temperatures in the intermediate superheat regime, the droplets and solid surface maintain only partial contact due to bubble nucleations at the solid–liquid interface. As in the case of low superheat, the droplets stick onto the solid surface during their entire lifetime. However, over the higher temperature range, the droplets become unstable and split into main and satellite droplets, each maintaining intermittent contact with the solid surface; this temperature range is sometimes called the transition region. Finally, if the surface temperature is increased beyond a critical value (the high superheat regime), a vapor layer formed beneath the droplets keeps them from contacting the solid surface. This mode of evaporation is commonly called the Leidenfrost phenomenon, and has been the subject of extensive studies [8–11].

In this paper, the heat transfer aspects of droplets evaporating in the low superheat regime will be studied. The analysis will cover the case of practical interests, in which a large number of droplets occupy a high fraction of the surface area. A consequence of high concentrations of droplets is that their thermal interactions may become significant, and the analyses based on an isolated droplet may no longer be appropriate. In this study, the single-droplet model of Sadhal and Plesset [2] (see Fig. 1) will be extended to include multiple-droplet systems, in which droplet thermal interactions will be dealt with rigorously. The model employed in this study consists of identical droplets in the form of a spherical cap arranged in a periodic array, either square or hexagonal, throughout the entire surface of a semi-infinite solid. Ignoring the effects of fluid motion inside the droplets, heat flow in the solid and liquid phases will be governed by steady-state conduction since the time scale of heat diffusion is much shorter than that of evaporation. At the solid–liquid interface, perfect thermal contact is assumed, and the usual conditions of continuity of temperature and heat flux across the interface hold. In view of the fact that the conductivity of vapor is much lower than that of solid or liquid, it is resonable to assume that heat diffusion across the solid–vapor or liquid–vapor interface is negligible. Thus, the solid–vapor interface is assumed to be impervious to heat flow, and all the heat crossing the solid–liquid interface diffuses towards the liquid–vapor interface, where it is taken up as the latent heat of evaporation. Saturation temperature will be assumed for the liquid–vapor interface. Later, the validity of the above assumptions will be discussed in greater detail.

NOMENCLATURE

$a, \dot{a}$ thickness of a liquid layer, time rate of change of a
a_ϑ, a_n equations (77), (81)–(83)
$A_n^{(0)}$ equations (30)–(33)
b distance between the reference droplet and its neighbor under consideration
c_p specific heat of droplet liquid
$C_n^{(m)}$ equations (57) and (64), Table 2
g gravitational acceleration
G_n Table 1
h heat transfer coefficient
$h_j, h_{j,6}, H_j$ equations (61), (62), (65) and (66)
h_ξ, h_η, h_ϕ metric coefficients of the toroidal coordinates (ξ, η, ϕ), equation (13)
k thermal conductivity
$\dot{m}$ rate of evaporation
N a positive integer
Nu Nusselt number, equation (1)
$q, \bar{q}$ heat flux, average heat flux at the solid surface
$q^{(0)}$ heat flux at the solid–liquid interface associated with $T_l^{(0)}$ and $T_s^{(0)}$
Q total rate of heat flow from the solid to one droplet
$Q^{(n)}$ rate of heat flow to a droplet associated with the pairs of $T_l^{(n)}$ and $T_s^{(n)}$
R radius of the base area of a droplet
$s_j, s_{j,4}, S_j$ equations (42), (43), (58) and (59)
t time
T temperature distribution
T_v a constant of the dimension of temperature
T_A temperature jump across the liquid–solid interface of droplet A
T_{AB} T_A due to droplet B
ΔT difference between the average temperature of solid surface and the liquid–vapor interfacial temperature
u velocity.

Greek symbols

α liquid thermal diffusivity
γ equation (88)
δ distance between a droplet and its closest neighbor
Δ equation (90)
η_0 $\vartheta + \pi$
ϑ droplet contact angle
κ fraction of the solid surface wetted by the droplets
λ liquid latent heat of evaporation
μ liquid-to-solid conductivity ratio
$\Xi^{(0)}, \Pi^{(0)}$ equations (22) and (23)
ρ mass density of droplet liquid
σ surface tension.

Coordinate systems

(x, y, z) rectangular coordinates
(ϱ, ϕ, z) cylindrical coordinates with the origin at the center of the base area of any one droplet under consideration and ϕ measured from the x-axis, Figs. 3 and 4
(r, ϕ, z) cylindrical coordinates, origin at the reference droplet, Figs. 3 and 4
(r, θ) polar coordinates with θ measured from the line joining the reference droplet and its neighbor under consideration, Fig. 2
(ξ, η, ϕ) toroidal coordinates.

Superscripts

(n) of order $(R/\delta)^n$; $T_l^{(n)}$ and $T_s^{(n)}$ superposed at the reference droplet will remove the nth-order term in T_A contributed by the nth-order expansions of the $T_s^{(0)}$ fields associated with the surrounding droplets
$(n+m)$ of order $(R/\delta)^{n+m}$; $T_l^{(n+m)}$ and $T_s^{(n+m)}$ superposed at the reference droplet will remove the $(n+m)$th-order term in T_A contributed by the mth-order expansions of the $T_s^{(n)}$ fields associated with the surrounding droplets
$(j+k+l)$ similar to $(n+m), j+k$ and l replacing n and m, respectively
$(n), j$ of order $(R/\delta)^n$ and angular dependence of $\cos j\phi$.

Subscripts

cond of conduction
conv of convection
evap of evaporation
l, s liquid, solid
$\kappa = 0$ ignoring droplet thermal interactions
H, S hexagonal array, square array.

Of main interest in this study is the calculation of heat transfer from the solid to the droplets and the corresponding heat transfer coefficient, h. In dimensionless form, it is given by the Nusselt number, Nu, defined by

$$Nu \equiv \frac{hR}{k_l} \equiv \frac{\bar{q}R}{k_l \Delta T}. \tag{1}$$

In equation (1) above, $\bar{q}$ is the average heat flux at the solid surface, k_l the thermal conductivity of the liquid,

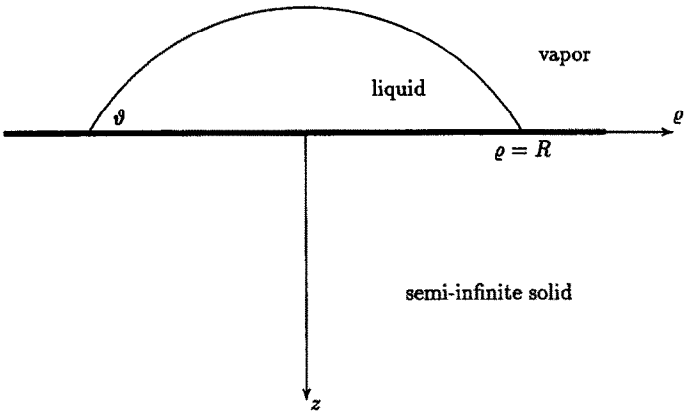

FIG. 1. An isolated droplet on the surface of a semi-infinite solid. The solid–liquid interface is a circular region of radius R.

R the base radius of the droplets, and ΔT the difference between the average temperature of the entire solid surface and the temperature of the liquid–vapor interface. By taking into account droplet thermal interactions, analytical expressions for the Nusselt number will be derived. We will also investigate the effect of array type, droplet concentration, droplet contact angle, and solid conductivity on the Nusselt number.

Admittedly, a periodic arrangement of identical droplets is rather specialized. A more realistic model would consist of a random arrangement of droplets with a spectrum of sizes. This random problem, however, is exceedingly complex, and at present, analytical methods to treat it are yet to be developed. The present study of identical droplets arranged regularly may, therefore, be regarded as a first step towards a comprehensive treatment of multiple-droplet systems.

2. GOVERNING EQUATIONS

For the model described above, the temperatures of the liquid and solid, T_l and T_s, respectively, satisfy Laplace's equation

$$\nabla^2 T_l = 0 \tag{2}$$

$$\nabla^2 T_s = 0. \tag{3}$$

At the solid surface, i.e. $z = 0$, the following boundary conditions hold:

$$\begin{cases} T_l = T_s \text{ and } k_l \dfrac{\partial T_l}{\partial z} = k_s \dfrac{\partial T_s}{\partial z}, \\ \qquad \text{solid–liquid interface} \\ \dfrac{\partial T_s}{\partial z} = 0, \\ \qquad \text{solid–vapor interface} \end{cases} \tag{4}$$

where k_l and k_s are the thermal conductivities of the liquid and solid, respectively. At the liquid–vapor interface, the boundary condition is that of constant temperature

$$T_l = \text{constant}. \tag{5}$$

Deep inside the solid, i.e. $z \to \infty$,

$$-k_s \frac{\partial T_s}{\partial z} = \text{constant}. \tag{6}$$

Due to the spatial periodicity of the mixed boundary conditions at the solid surface (Neumann condition over the non-wetted region, continuity conditions at the solid–liquid interface), a direct attempt to solve equations (2) and (3) for T_l and T_s will be very complicated. Therefore, an indirect approach based on the principle of linear superposition will be utilized. The method to be used is similar to that employed by Tio [12] in the study of thermal contact resistance. These methods are essentially an analytical corrective–iterative scheme.

The method of this paper consists of two fundamental steps. The first one is the analysis of a *single* droplet subject to various Dirichlet conditions at the solid–liquid interface. In spite of the geometrical complexity of a system composed of a spherical segment and a half-space, the problem is mathematically tractable with the use of the toroidal coordinates. The other step involves the calculation of the thermal interactions of the droplets. A consequence of these interactions is that the condition of temperature continuity at the solid–liquid interface has to be satisfied approximately. Nevertheless, accuracy up to $O(\kappa^{7/2})$, where κ is the fraction of the solid surface wetted by the droplets, is attained through a formal perturbation expansion. Laplace's equations along with the remaining boundary conditions are, however, satisfied exactly. In the ensuing sections, this method will be discussed in detail.

3. ANALYSIS OF A SINGLE DROPLET

The analysis of a single droplet on the surface of a semi-infinite solid (Fig. 1) was carried out by Sadhal and Plesset [2]. The discussion presented in this section represents a modification and extension of their analysis.

For an isolated droplet on the solid surface, the

governing equations and the boundary conditions are as follows:

$$\nabla^2 T_l^{(0)} = 0 \quad \text{in the liquid phase} \tag{7}$$

$$\nabla^2 T_s^{(0)} = 0 \quad \text{in the solid phase.} \tag{8}$$

At the liquid–vapor interface

$$T_l^{(0)} = T_v = \text{constant.} \tag{9}$$

At the solid surface

$$\begin{cases} T_l^{(0)} = T_s^{(0)} \text{ and } k_l \dfrac{\partial T_l^{(0)}}{\partial z} = k_s \dfrac{\partial T_s^{(0)}}{\partial z}, & \varrho < R \\ \dfrac{\partial T_s^{(0)}}{\partial z} = 0, & \varrho > R. \end{cases} \tag{10}$$

Deep inside the solid

$$T_s^{(0)} = 0. \tag{11}$$

It should be noted that the boundary condition in (11) is that of a uniform temperature instead of a uniform flux (see equation (6)). This is necessary because a uniform flux in the far field would result in an infinite amount of heat flow into the droplet. It should also be noted that T_v in (9) has a negative value since the far-field temperature of the solid is taken to be zero.

Exact solutions to (7)–(11) can be obtained by using the toroidal coordinates (ξ, η, ϕ), which are related to the cylindrical coordinates (ϱ, ϕ, z) by the formulas [13]

$$\varrho = \frac{R \sinh \xi}{\cosh \xi - \cos \eta}, \quad z = \frac{R \sin \eta}{\cosh \xi - \cos \eta} \tag{12}$$

where $0 \leqslant \xi < \infty$, $0 \leqslant \eta < 2\pi$. The metric coefficients are given by

$$h_\xi = h_\eta = \frac{R}{\cosh \xi - \cos \eta}, \quad h_\phi = \frac{R \sinh \xi}{\cosh \xi - \cos \eta}. \tag{13}$$

In this coordinate system, the solid–vapor interface corresponds to $\eta = 0$ and the solid–liquid interface is given by $\eta = \pi$. The edge of the droplet corresponds to $\xi = \infty$ and the z-axis to $\xi = 0$. The liquid–vapor interface is given by $\eta = \eta_0 = \pi + \vartheta$, where ϑ is the contact angle.

Under the coordinate transformation given by (12), the liquid region is defined by $0 \leqslant \xi < \infty$, $\pi < \eta < \eta_0$ and the semi-infinite solid region by $0 \leqslant \xi < \infty$, $0 < \eta < \pi$. Laplace's equation for these two regions (equations (7) and (8)) can be written as

$$\frac{\partial}{\partial \xi}\left(\frac{\sinh \xi}{\cosh \xi - \cos \eta} \frac{\partial T_{l,s}^{(0)}}{\partial \xi}\right) + \frac{\partial}{\partial \eta}\left(\frac{\sinh \xi}{\cosh \xi - \cos \eta} \frac{\partial T_{l,s}^{(0)}}{\partial \eta}\right) + \frac{1}{(\cosh \xi - \cos \eta) \sinh \xi} \frac{\partial^2 T_{l,s}^{(0)}}{\partial \phi^2} = 0. \tag{14}$$

The boundary conditions (9)–(11) are transformed into

$$\eta = \eta_0: \quad T_l^{(0)} = T_v \tag{15}$$

$$\eta = \pi: \quad k_l \frac{\partial T_l^{(0)}}{\partial \eta} = k_s \frac{\partial T_s^{(0)}}{\partial \eta} \tag{16}$$

$$T_l^{(0)} = T_s^{(0)} \tag{17}$$

$$\eta = 0: \quad \frac{\partial T_s^{(0)}}{\partial \eta} = 0 \tag{18}$$

$$(\xi, \eta) = (0, 0): \quad T_s^{(0)} = 0. \tag{19}$$

A convenient form for the temperature distribution is

$$T_l^{(0)} = T_v - T_v (2 \cosh \xi - 2 \cos \eta)^{1/2} \times \int_0^\infty \Xi^{(0)}(\tau) \sinh (\eta_0 - \eta) \tau P_{i\tau - 1/2}(\cosh \xi) \, d\tau \tag{20}$$

and

$$T_s^{(0)} = T_v (2 \cosh \xi - 2 \cos \eta)^{1/2} \times \int_0^\infty \Pi^{(0)}(\tau) \cosh \eta\tau P_{i\tau - 1/2}(\cosh \xi) \, d\tau \tag{21}$$

where $P_{i\tau - 1/2}$ is the Legendre function of the first kind, of complex degree

$$\Xi^{(0)}(\tau) = \frac{\sinh \pi\tau \operatorname{sech}^2 \pi\tau}{[\tanh \pi\tau \tanh \vartheta\tau + \mu] \cosh \vartheta\tau} \tag{22}$$

and

$$\Pi^{(0)}(\tau) = \frac{\mu \operatorname{sech}^2 \pi\tau}{[\tanh \pi\tau \tanh \vartheta\tau + \mu]}. \tag{23}$$

Here, $\mu = k_l/k_s$ is the liquid-to-solid conductivity ratio. In the course of obtaining the solution, the following integral expansion [13] is used:

$$\frac{1}{(2 \cosh \xi - 2 \cos \eta_p)^{1/2}} = \int_0^\infty \frac{\cosh (\pi - \eta_p)\tau}{\cosh \pi\tau} P_{i\tau - 1/2}(\cosh \xi) \, d\tau \qquad (0 < \eta_p < 2\pi). \tag{24}$$

The temperature of the dry solid area is needed in later analysis. To this end, it is expanded in the form

$$T_s^{(0)}(\eta = 0) = T_v \left[A_0^{(0)} + A_1^{(0)} \left(\frac{R}{\varrho}\right) + A_2^{(0)} \left(\frac{R}{\varrho}\right)^2 + A_3^{(0)} \left(\frac{R}{\varrho}\right)^3 + \cdots \right]. \tag{25}$$

It also follows from (21) that

$$T_s^{(0)}(\eta = 0) = T_v (2 \cosh \xi - 2)^{1/2} \times \int_0^\infty \Pi^{(0)}(\tau) P_{i\tau - 1/2}(\cosh \xi) \, d\tau. \tag{26}$$

Using the series expansion of ref. [13]

$$P_{i\tau-1/2}(\cosh\xi) = 1-\frac{(\tau^2+1/4)}{2\cdot(1!)^2}(\cosh\xi-1) + \frac{(\tau^2+1/4)(\tau^2+9/4)}{2^2\cdot(2!)^2}(\cosh\xi-1)^2 - \frac{(\tau^2+1/4)(\tau^2+9/4)(\tau^2+25/4)}{2^3\cdot(3!)^2}(\cosh\xi-1)^3+\cdots \quad (27)$$

which is valid for $\cosh\xi < 3$, equation (26) can be rewritten, after an extensive amount of algebra, as

$$T_s^{(0)}(\eta=0) = T_v\left(\frac{R}{\varrho}\right)\cdot 2\int_0^\infty \Pi^{(0)}(\tau)\,d\tau - T_v\left(\frac{R}{\varrho}\right)^3\cdot 2\int_0^\infty \Pi^{(0)}(\tau)\left(\tau^2-\frac{1}{4}\right)d\tau + T_v\left(\frac{R}{\varrho}\right)^5\cdot\int_0^\infty \Pi^{(0)}(\tau)\left(\frac{1}{2}\tau^4-\frac{7}{4}\tau^2+\frac{9}{32}\right)d\tau + T_v\left(\frac{R}{\varrho}\right)^7\cdot\int_0^\infty \Pi^{(0)}(\tau)\left(-\frac{1}{18}\tau^6+\frac{55}{72}\tau^4 - \frac{439}{288}\tau^2+\frac{25}{128}\right)d\tau+\cdots. \quad (28)$$

Comparing equations (25) and (28), we see that the temperature of the dry solid surface is given by

$$T_s^{(0)}(\eta=0) = T_v\left[A_1^{(0)}\left(\frac{R}{\varrho}\right)+A_3^{(0)}\left(\frac{R}{\varrho}\right)^3 + A_5^{(0)}\left(\frac{R}{\varrho}\right)^5+A_7^{(0)}\left(\frac{R}{\varrho}\right)^7+\cdots\right] \quad (29)$$

where

$$A_1^{(0)} = 2\int_0^\infty \Pi^{(0)}(\tau)\,d\tau \quad (30)$$

$$A_3^{(0)} = -2\int_0^\infty \Pi^{(0)}(\tau)\left(\tau^2-\frac{1}{4}\right)d\tau \quad (31)$$

$$A_5^{(0)} = \frac{1}{2}\int_0^\infty \Pi^{(0)}(\tau)\left(\tau^4-\frac{7}{2}\tau^2+\frac{9}{16}\right)d\tau \quad (32)$$

$$A_7^{(0)} = -\frac{1}{18}\int_0^\infty \Pi^{(0)}(\tau)\left(\tau^6-\frac{55}{4}\tau^4 + \frac{439}{16}\tau^2-\frac{225}{64}\right)d\tau. \quad (33)$$

Next, we calculate the total rate of heat flow $Q^{(0)}$ from the solid into the droplet. The heat flux at the solid–liquid interface is given by

$$q^{(0)} = -k_s\left[\frac{1}{h_\eta}\frac{\partial T_s^{(0)}}{\partial\eta}\right]_{\eta=\pi} = -\frac{k_s T_v}{2R}(2\cosh\xi+2)^{3/2} \times\int_0^\infty \tau\sinh\pi\tau\,\Pi^{(0)}(\tau)P_{i\tau-1/2}(\cosh\xi)\,d\tau. \quad (34)$$

Integrating (34) over the base area of the droplet, we obtain $Q^{(0)}$ as

$$Q^{(0)} = 2\pi\int_0^\infty q^{(0)}[h_\xi h_\phi]_{\eta=\pi}\,d\xi = -4\pi R k_s T_v\int_0^\infty \tau\sinh\pi\tau\,\Pi^{(0)}(\tau)\,d\tau \times\int_0^\infty \frac{\sinh\xi}{(2\cosh\xi+2)^{1/2}}P_{i\tau-1/2}(\cosh\xi)\,d\xi. \quad (35)$$

The inner integral in (35) is the zeroth-order Mehler–Fock transform of $(2\cosh\xi+2)^{-1/2}$, and is given in ref. [14] as $1/\tau\sinh\pi\tau$. Thus,

$$Q^{(0)} = -2\pi R k_s T_v A_1^{(0)}. \quad (36)$$

4. TWO-DROPLET INTERACTIONS

While the toroidal coordinate system fits nicely into the geometry involving one droplet on the surface of a semi-infinite solid, the presence of another droplet introduces serious complications. For one thing, there exists no orthogonal coordinate system which fits into the geometry of two droplets. Thus, both the toroidal and cylindrical coordinate systems are employed in this paper.

Consider two droplets, labeled A and B, evaporating on a solid surface as shown in Fig. 2. In the limit of $b\to\infty$, both droplets have no thermal effect on each other. This suggests that, for finite b, we may start the two-droplet analysis with the temperature distributions given by the pair of (20) and (21). Thus, to each of the two droplets, we superpose a pair of $T_1^{(0)}$ and $T_s^{(0)}$, and consider the effect of one droplet on the other.

The temperature distribution over contact area A, i.e. the base area of droplet A, contributed by the $T_s^{(0)}$ associated with droplet B is, according to equation (29), given by

$$T_{AB} = A_1^{(0)}T_v\left(\frac{R}{\varrho}\right)+A_3^{(0)}T_v\left(\frac{R}{\varrho}\right)^3 + A_5^{(0)}T_v\left(\frac{R}{\varrho}\right)^5+A_7^{(0)}T_v\left(\frac{R}{\varrho}\right)^7+\cdots. \quad (37)$$

Using the Legendre polynomial identity

$$\left(\frac{R}{\varrho}\right) = \left(\frac{R}{b}\right)\sum_{n=0}^\infty\left(\frac{r}{b}\right)^n P_n(\cos\theta) \quad (38)$$

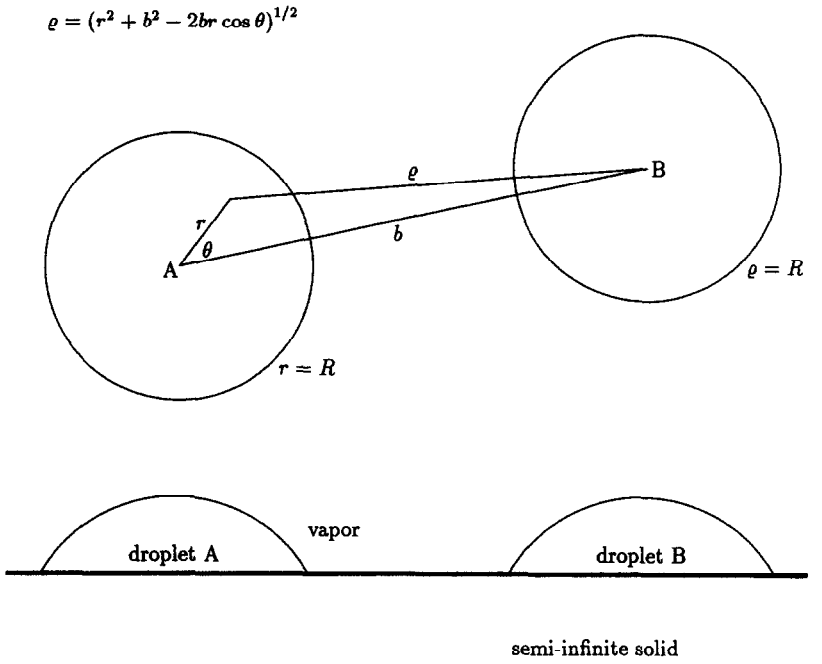

FIG. 2. Two droplets of base radius R on the surface of a semi-infinite solid. The two circular regions are the wetted areas of the solid surface.

and its derivatives

$$\left(\frac{R}{\varrho}\right)^m = \frac{1}{1\cdot 3\ldots(m-2)}\left(\frac{R}{b}\right)^m \times \sum_{n=(m-1)/2}^{\infty}\left(\frac{r}{b}\right)^{n-(m-1)/2}\left.\frac{\mathrm{d}^{(m-1)/2}P_n(x)}{\mathrm{d}x^{(m-1)/2}}\right|_{x=\cos\theta} \tag{39}$$

where $m = 3, 5, 7, \ldots$, we expand equation (37) about the center of contact area A in terms of the cylindrical polar coordinates (r, θ), and obtain

$$\begin{aligned}
T_{AB} = {} & A_1^{(0)}T_v\left(\frac{R}{b}\right) + \left[A_1^{(0)}\left(\frac{r}{R}\right)\cos\theta\right]T_v\left(\frac{R}{b}\right)^2 \\
& + \left[A_3^{(0)} + \frac{1}{4}A_1^{(0)}(3\cos 2\theta + 1)\left(\frac{r}{R}\right)^2\right]T_v\left(\frac{R}{b}\right)^3 \\
& + \left[3A_3^{(0)}\left(\frac{r}{R}\right)\cos\theta + \frac{1}{8}A_1^{(0)}(5\cos 3\theta\right. \\
& \left. + 3\cos\theta)\left(\frac{r}{R}\right)^3\right]T_v\left(\frac{R}{b}\right)^4 \\
& + \left[A_5^{(0)} + \frac{3}{4}A_3^{(0)}(5\cos 2\theta + 3)\left(\frac{r}{R}\right)^2\right. \\
& + \frac{1}{64}A_1^{(0)}(35\cos 4\theta \\
& \left. + 20\cos 2\theta + 9)\left(\frac{r}{R}\right)^4\right]T_v\left(\frac{R}{b}\right)^5 \\
& + \left[5A_5^{(0)}\left(\frac{r}{R}\right)\cos\theta + \frac{5}{8}A_3^{(0)}(7\cos 3\theta + 9\cos\theta)\left(\frac{r}{R}\right)^3\right. \\
& + \frac{1}{128}A_1^{(0)}(63\cos 5\theta + 35\cos 3\theta \\
& \left. + 30\cos\theta)\left(\frac{r}{R}\right)^5\right]T_v\left(\frac{R}{b}\right)^6 \\
& + \left[A_7^{(0)} + \frac{5}{4}A_5^{(0)}(7\cos 2\theta + 5)\left(\frac{r}{R}\right)^2\right. \\
& + \frac{15}{64}A_3^{(0)}(21\cos 4\theta + 28\cos 2\theta + 15)\left(\frac{r}{R}\right)^4 \\
& + \frac{1}{512}A_1^{(0)}(231\cos 6\theta + 126\cos 4\theta \\
& \left. + 105\cos 2\theta + 50)\left(\frac{r}{R}\right)^6\right]T_v\left(\frac{R}{b}\right)^7 \\
& + \left[7A_7^{(0)}\left(\frac{r}{R}\right)\cos\theta + \frac{35}{8}A_5^{(0)}(3\cos 3\theta + 5\cos\theta)\left(\frac{r}{R}\right)^3\right. \\
& + \frac{21}{128}A_3^{(0)}(33\cos 5\theta + 45\cos 3\theta + 50\cos\theta)\left(\frac{r}{R}\right)^5 \\
& + \frac{1}{1024}A_1^{(0)}(429\cos 7\theta + 231\cos 5\theta \\
& \left. + 189\cos 3\theta + 175\cos\theta)\left(\frac{r}{R}\right)^7\right]T_v\left(\frac{R}{b}\right)^8 + O\left(\frac{R}{b}\right)^9.
\end{aligned} \tag{40}$$

While the pair of $T_l^{(0)}$ and $T_s^{(0)}$ associated with droplet A satisfies the continuity of temperature and heat flux at the solid–liquid interface of A, the presence of T_{AB} destroys the continuity of temperature at the base area of droplet A. In effect, T_{AB} given by (40) represents a temperature jump at the solid–liquid interface of A; this discontinuity in temperature is caused by droplet B. The continuity of heat flux, however, is preserved since $T_s^{(0)}$ associated with droplet B satisfies the no-flux condition around B. To restore the continuity of temperature, we must superpose additional temperature fields at each droplet. Thus, $T_l^{(0)}$ and $T_s^{(0)}$ are actually the leading-order terms of the series of temperature distributions in the liquid and solid phases, respectively.

In the next two sections, this basic principle will be applied to systems of multiple droplets arranged in a square array and a hexagonal array, respectively. Due to the symmetry of the droplet arrangements, the multiple-droplet problem is actually simpler than the two-droplet model.

5. SQUARE ARRAY OF DROPLETS

To analyze the problem of droplets arranged in a square array, consider a large square of sides $(2N+1)\delta$ on the surface of the solid and the $(2N+1)^2$ droplets inside it, as shown in Fig. 3. Later, the limit of $N \to \infty$ will be taken, thus recovering the infinite number of droplets in a square array arrangement. The droplet at the center of the square, labeled A, is taken as the reference droplet.

Now, at each droplet inside the square, we superpose a pair of the leading fields $T_l^{(0)}$ and $T_s^{(0)}$. Then, the temperature jump at the solid–liquid interface of droplet A is given by

$$
\begin{aligned}
T_A = {} & A_1^{(0)} T_v s_1(N)\left(\frac{R}{\delta}\right) \\
& + \left[A_3^{(0)} + \frac{1}{4} A_1^{(0)}\left(\frac{r}{R}\right)^2\right] T_v s_3(N)\left(\frac{R}{\delta}\right)^3 \\
& + \left[\left\{A_5^{(0)} + \frac{9}{4} A_3^{(0)}\left(\frac{r}{R}\right)^2 + \frac{9}{64} A_1^{(0)}\left(\frac{r}{R}\right)^4\right\} s_5(N)\right. \\
& \left. + \left\{\frac{35}{64} A_1^{(0)}\left(\frac{r}{R}\right)^4 \cos 4\phi\right\} s_{5,4}(N)\right] T_v\left(\frac{R}{\delta}\right)^5 \\
& + \left[\left\{A_7^{(0)} + \frac{25}{4} A_5^{(0)}\left(\frac{r}{R}\right)^2 + \frac{225}{64} A_3^{(0)}\left(\frac{r}{R}\right)^4\right.\right. \\
& \left. + \frac{50}{512} A_1^{(0)}\left(\frac{r}{R}\right)^6\right\} s_7(N) + \left\{\frac{315}{64} A_3^{(0)}\left(\frac{r}{R}\right)^4\right. \\
& \left.\left. + \frac{126}{512} A_1^{(0)}\left(\frac{r}{R}\right)^6\right\} s_{7,4}(N) \cos 4\phi\right] T_v\left(\frac{R}{\delta}\right)^7 \\
& + O\left(\frac{R}{\delta}\right)^9
\end{aligned}
\tag{41}
$$

where

$$
s_j(N) = (4+2^{(4-j)/2}) \sum_{n=1}^{N} \frac{1}{n^j} + 8 \sum_{n=1}^{N-1} \sum_{m=n+1}^{N} \frac{1}{(m^2+n^2)^{j/2}} \tag{42}
$$

$$
s_{j,4}(N) = (4-2^{(4-j)/2}) \sum_{n=1}^{N} \frac{1}{n^j} + 8 \sum_{n=1}^{N-1} \sum_{m=n+1}^{N} \frac{1}{(m^2+n^2)^{j/2}} \left[2\left(\frac{m^2-n^2}{m^2+n^2}\right)^2 - 1\right]. \tag{43}
$$

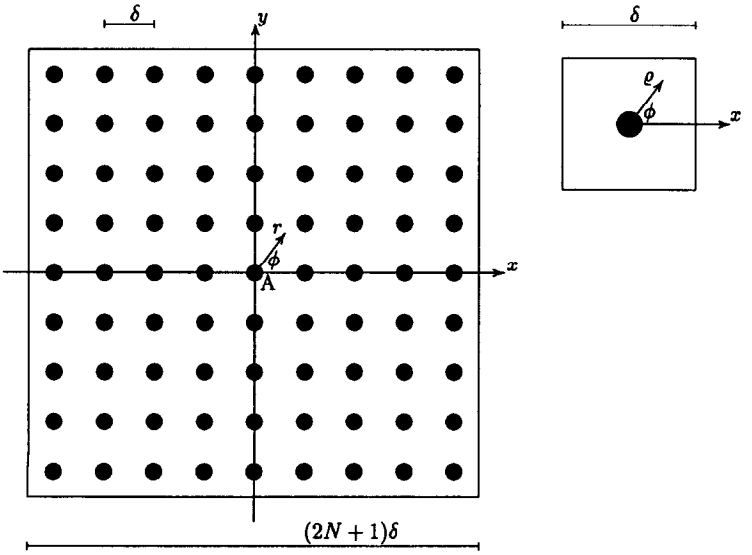

FIG. 3. A square array of droplets on the surface of a semi-infinite solid. The solid–liquid interfacial regions of radius R are shown. The reference droplet, A, is located at the center of the square. A typical unit cell of the array is also shown.

Equation (41) represents the summation of (40) over each of the droplets inside the square, A being excluded. The single sums in equations (42) and (43) correspond to the summation over all the droplets on the axes and the diagonals of the square, excluding A, while the double sums represent those located off the axes or diagonals. Since the droplets surrounding A are arranged in four-fold symmetry, all the θ-dependent terms in equation (40), except those of the type $\cos 4\theta$, $\cos 8\theta$, etc., cancel out. For $N \to \infty$, $s_1(N)$ becomes unbounded. However, this problem can be taken care of quite easily [12].

Now, we are going to remove the temperature jump T_A, equation (41), from the solid–liquid interface of the reference droplet in sequential orders of (R/δ). The first-order term in (41) can be removed by adding $T_{l,S}^{(1)}$ and $T_{s,S}^{(1)}$ to droplet A. For an isolated droplet (Fig. 1), these first-order fields satisfy Laplace's equation

$$\nabla^2 T_{l,S}^{(1)} = 0, \quad 0 \leqslant \xi < \infty, \ \pi < \eta < \eta_0 \tag{44}$$

$$\nabla^2 T_{s,S}^{(1)} = 0, \quad 0 \leqslant \xi < \infty, \ 0 < \eta < \pi. \tag{45}$$

The boundary conditions are

$$\eta = \eta_0: \ T_{l,S}^{(1)} = \text{constant} \tag{46}$$

$$\eta = \pi: \ k_l \frac{\partial T_{l,S}^{(1)}}{\partial \eta} = k_s \frac{\partial T_{s,S}^{(1)}}{\partial \eta} \tag{47}$$

$$T_{l,S}^{(1)} = T_{s,S}^{(1)} + A_1^{(0)} T_v s_1(N) \left(\frac{R}{\delta}\right) \tag{48}$$

$$\eta = 0: \ \frac{\partial T_{s,S}^{(1)}}{\partial \eta} = 0 \tag{49}$$

$$(\xi, \eta) = (0, 0): \ T_{s,S}^{(1)} = 0. \tag{50}$$

The solution to (44)–(50) is easily determined to be

$$T_{l,S}^{(1)} = A_1^{(0)} T_v s_1(N) \left(\frac{R}{\delta}\right) \tag{51}$$

and

$$T_{s,S}^{(1)} = 0. \tag{52}$$

The total rate of heat flow $Q_S^{(1)}$ from the solid into the droplet is given by

$$Q_S^{(1)} = 0. \tag{53}$$

With $T_{l,S}^{(1)}$ and $T_{s,S}^{(1)}$ added to the reference droplet, the first-order term in (41) is now deleted. Since each of the droplets in an infinite regular array has the same temperature distribution, the same pair of $T_{l,S}^{(1)}$ and $T_{s,S}^{(1)}$ must also be added to each of the remaining droplets inside the square. However, these pairs of $T_{l,S}^{(1)}$ and $T_{s,S}^{(1)}$ will not introduce any temperature jumps to the solid–liquid interface of droplet A. The third-order correction to (41) is achieved by adding a pair of $T_{l,S}^{(3)}$ and $T_{s,S}^{(3)}$ to droplet A. For an isolated droplet on the surface of the solid (Fig. 1), these temperature distributions satisfy (44)–(50), condition (48) being replaced by

$$T_{l,S}^{(3)} = T_{s,S}^{(3)} + \left[A_3^{(0)} + \frac{1}{4} A_1^{(0)} \frac{\sinh^2 \xi}{(\cosh \xi + 1)^2}\right] T_v s_3(N) \left(\frac{R}{\delta}\right)^3. \tag{54}$$

The derivation of the temperature distributions $T_{l,S}^{(3)}$ and $T_{s,S}^{(3)}$ is similar to that of $T_l^{(0)}$ and $T_s^{(0)}$, and will not be presented here. A detailed treatment of this is given in ref. [12]. While the third-order pair of $T_{l,S}^{(3)}$ and $T_{s,S}^{(3)}$ added to droplet A deletes the discontinuity of temperature caused by the third-order term in (41), the same pairs added to the remaining droplets will introduce a fourth-order temperature jump to the solid–liquid interface of A. To move the temperature jump to $O(R/\delta)^8$, we superpose a few pairs of temperature fields at droplet A (and each of the rest) on the existing $T_l^{(0)}$, $T_s^{(0)}$, $T_{l,S}^{(1)}$, $T_{s,S}^{(1)}$, $T_{l,S}^{(3)}$, and $T_{s,S}^{(3)}$. These additional temperature distributions are $T_{l,S}^{(3+1)}$, $T_{s,S}^{(3+1)}$, $T_{l,S}^{(5)}$, $T_{s,S}^{(5)}$, $T_{l,S}^{(5),4}$, $T_{s,S}^{(5),4}$, $T_{l,S}^{(5+1)}$, $T_{s,S}^{(5+1)}$, $T_{l,S}^{(3+3)}$, $T_{s,S}^{(3+3)}$, $T_{l,S}^{(3+3+1)}$, $T_{s,S}^{(3+3+1)}$, $T_{l,S}^{(7)}$, $T_{s,S}^{(7)}$, $T_{l,S}^{(7),4}$, $T_{s,S}^{(7),4}$, $T_{l,S}^{(7+1)}$, and $T_{s,S}^{(7+1)}$, which are also given in ref. [12].

In summary, by superposing the temperature fields $T_l^{(0)}$, $T_s^{(0)}$, $T_{l,S}^{(1)}$, $T_{s,S}^{(1)}$, $T_{l,S}^{(3)}$, $T_{s,S}^{(3)}$, $T_{l,S}^{(3+1)}$, $T_{s,S}^{(3+1)}$, $T_{l,S}^{(5)}$, $T_{s,S}^{(5)}$, $T_{l,S}^{(5),4}$, $T_{s,S}^{(5),4}$, $T_{l,S}^{(5+1)}$, $T_{s,S}^{(5+1)}$, $T_{l,S}^{(3+3)}$, $T_{s,S}^{(3+3)}$, $T_{l,S}^{(3+3+1)}$, $T_{s,S}^{(3+3+1)}$, $T_{l,S}^{(7)}$, $T_{s,S}^{(7)}$, $T_{l,S}^{(7),4}$, $T_{s,S}^{(7),4}$, $T_{l,S}^{(7+1)}$, and $T_{s,S}^{(7+1)}$ at each of the droplets inside the square, we obtain the temperature jump at the solid–liquid interface of the reference droplet as

$$T_A = O\left(\frac{R}{\delta}\right)^8. \tag{55}$$

Furthermore, T_A remains finite as $N \to \infty$. The Nusselt number, corresponding to these temperature distributions, is given by

$$\begin{aligned}\frac{\kappa}{Nu} = {} & \frac{\mu}{2A_1^{(0)}} + \frac{\mu}{2} C_1^{(4)} \kappa^{1/2} \\ & + \frac{\mu}{2A_1^{(0)}} [2A_3^{(0)}] C_3^{(4)} \kappa^{3/2} \\ & + \frac{\mu}{2A_1^{(0)}} \left[2A_5^{(0)} + 9 \frac{A_3^{(0)} A_3^{(0)}}{A_1^{(0)}}\right] C_5^{(4)} \kappa^{5/2} \\ & - \frac{\mu}{2A_1^{(0)}} [\tfrac{1}{4} A_1^{(0)} A_1^{(0)} - 3A_1^{(0)} A_3^{(0)} \\ & + 4A_1^{(0)} A_5^{(0)} - A_3^{(0)} A_3^{(0)}] C_3^{(4)} C_3^{(4)} \kappa^{6/2} \\ & + \frac{\mu}{2A_1^{(0)}} \left[2A_7^{(0)} + 50 \frac{A_3^{(0)} A_5^{(0)}}{A_1^{(0)}}\right] C_7^{(4)} \kappa^{7/2} \\ & + O(\kappa^{8/2}).\end{aligned} \tag{56}$$

In equation (56) above, κ is the area fraction of the solid surface wetted by the droplets and is equal to $\pi R^2/\delta^2$. We have also used the notation of

$$C_n^{(4)} = \frac{S_n}{\pi^{n/2}} \tag{57}$$

where the superscript (4) signifies summations over a square array, and

$$S_1 = \lim_{N\to\infty}\left[s_1(N) - (8N+4)\ln\tan\frac{3\pi}{8}\right] \quad (58)$$

$$S_j = \lim_{N\to\infty} s_j(N), \quad j = 3,5,\ldots. \quad (59)$$

By numerical evaluation, these various array sums are found to be $S_1 = -3.90026$, $S_3 = 9.03362$, $S_5 = 5.09026$, and $S_7 = 4.42312$.

For the sake of brevity, we have left out the lengthy development leading to formula (56). The interested reader may refer to ref. [12] for the detailed treatment. Here, it suffices to point out that the right-hand side of equation (56) is *the* first six terms of the complete power series expansion in $\kappa^{1/2}$.

6. HEXAGONAL ARRAY OF DROPLETS

The analysis of the problem of a hexagonal array of droplets is similar to that of a square array. First, we consider a large hexagon of sides $(N+1/2)\delta$ on the solid surface and the $(3N^2+3N+1)$ droplets inside the hexagon (Fig. 4). Later, we let $N\to\infty$, and recover an infinite number of droplets arranged in a hexagonal array.

At each of the droplets inside the hexagon, we superpose a pair of the leading-order temperature fields $T_1^{(0)}$ and $T_s^{(0)}$. Then, the temperature jump at the solid–liquid interface of droplet A located at the center of the hexagon is

$$T_A = A_1^{(0)}T_v h_1(N)\left(\frac{R}{\delta}\right) + \left[A_3^{(0)} + \frac{1}{4}A_1^{(0)}\left(\frac{r}{R}\right)^2\right]T_v h_3(N)\left(\frac{R}{\delta}\right)^3 + \left[A_5^{(0)} + \frac{9}{4}A_3^{(0)}\left(\frac{r}{R}\right)^2 + \frac{9}{64}A_1^{(0)}\left(\frac{r}{R}\right)^4\right]T_v h_5(N)\left(\frac{R}{\delta}\right)^5 + \left[\left\{A_7^{(0)} + \frac{25}{4}A_5^{(0)}\left(\frac{r}{R}\right)^2 + \frac{225}{64}A_3^{(0)}\left(\frac{r}{R}\right)^4 + \frac{50}{512}A_1^{(0)}\left(\frac{r}{R}\right)^6\right\}h_7(N) + \left\{\frac{231}{512}A_1^{(0)}\left(\frac{r}{R}\right)^6\cos 6\phi\right\}h_{7,6}(N)\right]T_v\left(\frac{R}{\delta}\right)^7 + O\left(\frac{R}{\delta}\right)^9 \quad (60)$$

where

$$h_j(N) = 6\sum_{n=1}^{N}\frac{1}{n^j} + 6\sum_{n=1}^{N-1}\sum_{m=n+1}^{N}\frac{1}{(m^2-mn+n^2)^{j/2}} \quad (61)$$

$$h_{j,6}(N) = 6\sum_{n=1}^{N}\frac{1}{n^j} + 6\sum_{n=1}^{N-1}\sum_{m=n+1}^{N}\frac{1}{(m^2-mn+n^2)^{j/2}} \times\left[1 - \frac{27}{2}\frac{m^2n^2(m-n)^2}{(m^2-mn+n^2)^3}\right]. \quad (62)$$

Equation (60) represents the summation of (40) over each of the droplets inside the hexagon, A being excluded. The single sums in (61) and (62) correspond to summing over the droplets located on the diagonals of the hexagon while the double sums represent the remaining droplets. Of all the θ-dependent terms in (40), only those of $\cos 6\theta$, $\cos 12\theta$, etc. remain in equation (60) since the droplets surrounding A are

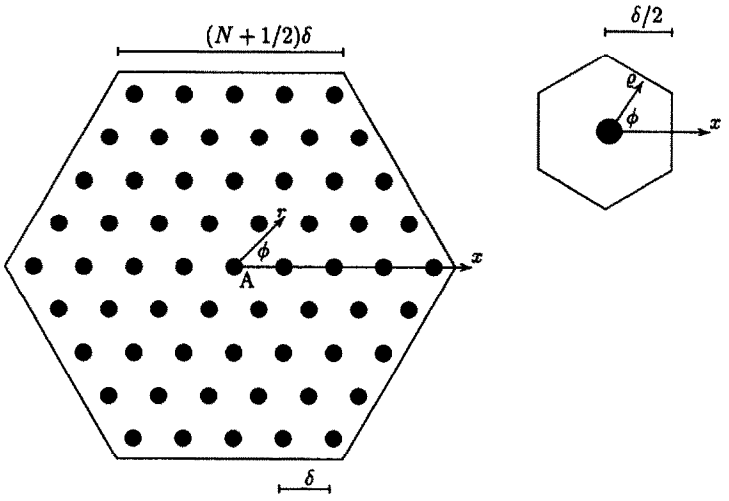

FIG. 4. A hexagonal array of droplets of base radius R on the surface of a semi-infinite solid. The solid–liquid interfacial areas are shown. The droplet at the center of the hexagon, labeled A, is the reference droplet. A typical unit cell is also shown.

arranged in six-fold symmetry. Like $s_1(N)$, $h_1(N)$ becomes unbounded as $N \to \infty$.

Equation (60) shows that temperature discontinuity at the solid–liquid interface of droplet A occurs at $O(R/\delta)$. To move it to $O(R/\delta)^8$, we need additional pairs of temperature fields for each of the droplets inside the hexagon. These temperature distributions are: $T_{l,H}^{(1)}$, $T_{s,H}^{(1)}$, $T_{l,H}^{(3)}$, $T_{s,H}^{(3)}$, $T_{l,H}^{(3+1)}$, $T_{s,H}^{(3+1)}$, $T_{l,H}^{(5)}$, $T_{s,H}^{(5)}$, $T_{l,H}^{(5+1)}$, $T_{s,H}^{(5+1)}$, $T_{l,H}^{(3+3)}$, $T_{s,H}^{(3+3)}$, $T_{l,H}^{(3+3+1)}$, $T_{s,H}^{(3+3+1)}$, $T_{l,H}^{(7)}$, $T_{s,H}^{(7)}$, $T_{l,H}^{(7),6}$, $T_{s,H}^{(7),6}$, $T_{l,H}^{(7+1)}$, and $T_{s,H}^{(7+1)}$. Again, the reader is referred to ref. [12] for the derivation of these temperature distributions.

After superposing the temperature distributions $T_l^{(0)}$, $T_s^{(0)}$, $T_{l,H}^{(1)}$, $T_{s,H}^{(1)}$, $T_{l,H}^{(3)}$, $T_{s,H}^{(3)}$, $T_{l,H}^{(3+1)}$, $T_{s,H}^{(3+1)}$, $T_{l,H}^{(5)}$, $T_{s,H}^{(5)}$, $T_{l,H}^{(5+1)}$, $T_{s,H}^{(5+1)}$, $T_{l,H}^{(3+3)}$, $T_{s,H}^{(3+3)}$, $T_{l,H}^{(3+3+1)}$, $T_{s,H}^{(3+3+1)}$, $T_{l,H}^{(7)}$, $T_{s,H}^{(7)}$, $T_{l,H}^{(7),6}$, $T_{s,H}^{(7),6}$, $T_{l,H}^{(7+1)}$, and $T_{s,H}^{(7+1)}$ at each droplet inside the hexagon, we obtain the temperature jump at the solid–liquid interface of droplet A as

$$T_A = O\left(\frac{R}{\delta}\right)^8. \tag{63}$$

The Nusselt number is identical to (56), except that the array sums $C_n^{(4)}$ are replaced by the corresponding $C_n^{(6)}$. For a hexagonal array,

$$C_n^{(6)} = \left(\frac{\sqrt{3}}{2}\right)^{n/2} \frac{H_n}{\pi^{n/2}}. \tag{64}$$

The array sums H_n are in turn given by

$$H_1 = \lim_{N\to\infty} [h_1(N) - (6N+3)\ln 3] \tag{65}$$

$$H_j = \lim_{N\to\infty} h_j(N), \quad j = 3, 5, \ldots. \tag{66}$$

These array sums are evaluated numerically to be $H_1 = -4.21342$, $H_3 = 11.0342$, $H_5 = 6.76190$, and $H_7 = 6.19524$. For a hexagonal arrangement, the area fraction of the solid surface wetted by the droplets, κ, is equal to $2\pi R^2/\delta^2\sqrt{3}$.

7. RESULTS AND DISCUSSION

7.1. *Validity of assumptions*

Dropwise evaporation is a complex phenomenon. A complete formulation of the problem must include all three transport mechanisms of momentum, heat, and mass. In addition, it is generally a transient problem due to the changing solid–liquid and liquid–vapor interfaces. However, as far as heat transfer in the low superheat regime is concerned, the model of the present study is adequate, as shown by the examination below of the mechanisms involved, their relative importance, and the validity of the assumptions.

Of the three phases, only the solid and liquid have been incorporated into the analysis of the present study. The vapor phase is thermally decoupled from the solid by the assumption of adiabatic solid–vapor interface. At the liquid–vapor interface, liquid saturation temperature is assumed, following Plesset's results [15, 16], which show that the temperature of an evaporating liquid surface can be approximated with that of the surrounding vapor.

In the liquid phase, three types of motion can be identified: evaporation-induced flow, liquid motion due to the buoyancy effect, and surface-tension-driven flow. To see the effect of evaporation-induced liquid motion on heat transfer, suppose first that conduction is the dominant mode of heat transfer. A conductive heat flux of q_{cond} crossing the solid–liquid interface and diffusing towards the liquid–vapor interface will generate a vapor mass flux $\dot{m}$ leaving the droplets. In terms of order of magnitude,

$$\dot{m} \sim \frac{q_{cond}}{\lambda}. \tag{67}$$

The mass flux $\dot{m}$ will in turn generate liquid motion with velocities u of order of magnitude of

$$u \sim \frac{q_{cond}}{\lambda\rho}. \tag{68}$$

The convective flux corresponding to u is then given by

$$q_{conv} \sim \rho c_p u \Delta T \sim \frac{c_p \Delta T}{\lambda} q_{cond}. \tag{69}$$

For water at 100°C and ΔT of 5°C, we then have $q_{conv} \sim 0.01 q_{cond}$, and the effect of evaporation-induced convection can be ignored. Since the solid–liquid interface of an evaporating sessile droplet is warmer than its free surface, the possibility of buoyancy-driven convection exists. Furthermore, fluid motion within the droplet may also be induced by surface-tension gradients along its free surface. In this regard, stability analyses have been carried out recently by Yang and co-workers [17, 18]. From the analyses of Pearson [19] and Nield [20], one can conclude that for thin liquid layers, thermocapillary effects are more important than buoyancy. For water with thickness of 1 mm or less, the onset of cellular motion can be attributed to thermocapillary effects rather than buoyancy. Even then, with the high surface tension of water such motion is rather weak. In a study of condensing droplets, Lorenz and Mikic [21] showed that the effects of thermocapillary flow on heat transfer were insignificant. The fact that the contribution from convection, either driven by the buoyancy effect or surface-tension gradients, to heat transfer is negligible is primarily due to the large conductive heat fluxes. For example, consider a system of water droplets evaporating on stainless steel in the neighborhood of the boiling point of water. Then, neglecting droplet thermal interactions, the average heat flux crossing the solid–liquid interface of a droplet with $\vartheta = \pi/3$, $R = 0.5$ mm, and $\Delta T = 5$°C is about 90 kW m^{-2} (see equation (89)).

Thus, in heat transfer analyses of dropwise evaporation, only conduction needs to be considered, since radiation effects are generally negligible. Furthermore, transient effects in conduction can be ignored,

since the time it takes a droplet to change by an amount comparable to its original size is much longer than that needed by heat diffusion. Consider, for simplicity, a liquid layer of thickness a evaporating on a solid surface. Let ΔT be the difference in temperature between the solid and the free surface of the liquid layer. Then, the conductive heat flux flowing into the liquid is given by

$$q_{\text{cond}} \sim \frac{k_l \Delta T}{a}. \tag{70}$$

Corresponding to q_{cond}, the rate of change of the film thickness is

$$\dot{a} \sim -\frac{k_l \Delta T}{\rho \lambda a}. \tag{71}$$

Thus, the time it takes to evaporate the layer by an amount comparable to its original thickness is given by

$$t_{\text{evap}} \sim \frac{a}{-\dot{a}} \sim \frac{a^2 \rho \lambda}{k_l \Delta T}. \tag{72}$$

On the other hand, the time scale of heat diffusion is given by

$$t_{\text{cond}} \sim \frac{a^2}{\alpha} \tag{73}$$

where α is the liquid thermal diffusivity. Thus,

$$t_{\text{cond}} \sim \frac{c_p \Delta T}{\lambda} t_{\text{evap}} \sim 0.01 t_{\text{evap}} \tag{74}$$

for water at 100°C and ΔT of 5°C, and the transient effects in conduction caused by evaporation can be ignored.

Another assumption for the model of the present study is that the droplets have the shape of a spherical cap. For droplets of base radius of 0.5 mm or less, the assumed shape is quite reasonable because the effects of surface tension are dominant over those of gravity. In fact, the Bond number, $Bo \equiv \rho g R^2/\sigma$, is only about 0.04 for water droplets of base radius 0.5 mm.

7.2. *Asymptotic expansions for* $\mu \ll 1$

As stated earlier, the main objective of this study is the derivation of the Nusselt number as a function of droplet arrangement, droplet concentration, droplet contact angle, and solid thermal conductivity. For $\vartheta \neq 0$ and $\mu \ll 1$, analytical estimates for the integrals in (30)–(33) can be obtained. For $\mu \to 0$, the dominant contribution to the integral in (30) takes place near $\tau = 0$. Therefore, we can replace $\tanh \vartheta\tau$ with $(\vartheta/\pi)\tanh \pi\tau$. Thus, we write

$$A_1^{(0)} = 2\mu \int_0^\infty \frac{\operatorname{sech}^2 \pi\tau}{\mu + (\vartheta/\pi)\tanh^2 \pi\tau}\, d\tau + 2\mu \int_0^\infty \frac{\operatorname{sech}^2 \pi\tau[(\vartheta/\pi)\tanh \pi\tau - \tanh \vartheta\tau]\tanh \pi\tau}{[\tanh \pi\tau \tanh \vartheta\tau + \mu] \times [\mu + (\vartheta/\pi)\tanh^2 \pi\tau]}\, d\tau, \tag{75}$$

where the first term on the right-hand side represents the leading-order approximation to $A_1^{(0)}$ and the second the correction term. Also, the first term can be evaluated exactly and a detailed calculation yields $2(\mu/\vartheta\pi)^{1/2} \arctan (\vartheta/\mu\pi)^{1/2}$. The second term is of $O(\mu)$; it in turn can be written as an order-μ term plus a higher-order correction. Thus, after some algebra, we obtain

$$A_1^{(0)} \sim \left(\frac{\pi\mu}{\vartheta}\right)^{1/2} + 2a_\vartheta \left(\frac{\pi\mu}{\vartheta}\right)^{2/2} - \frac{1}{2}\left[\frac{\vartheta^2}{\pi^2} - 1\right]\left(\frac{\pi\mu}{\vartheta}\right)^{3/2} + O\left[\left(\frac{\pi\mu}{\vartheta}\right)^{4/2}\right] \tag{76}$$

where

$$a_\vartheta = \int_0^\infty \frac{\operatorname{sech}^2 \pi\tau[(\vartheta/\pi)\tanh \pi\tau - \tanh \vartheta\tau]}{\tanh^2 \pi\tau \tanh \vartheta\tau}\, d\tau - \frac{1}{\pi}. \tag{77}$$

Similarly,

$$A_3^{(0)} \sim \frac{1}{4}\left(\frac{\pi\mu}{\vartheta}\right)^{1/2} + \left(\frac{1}{2}a_\vartheta - a_2\right)\left(\frac{\pi\mu}{\vartheta}\right)^{2/2} + O\left[\left(\frac{\pi\mu}{\vartheta}\right)^{3/2}\right] \tag{78}$$

$$A_5^{(0)} \sim \frac{9}{64}\left(\frac{\pi\mu}{\vartheta}\right)^{1/2} + \left(\frac{9}{32}a_\vartheta - a_4\right)\left(\frac{\pi\mu}{\vartheta}\right)^{2/2} + O\left[\left(\frac{\pi\mu}{\vartheta}\right)^{3/2}\right] \tag{79}$$

$$A_7^{(0)} \sim \frac{25}{256}\left(\frac{\pi\mu}{\vartheta}\right)^{1/2} + \left(\frac{25}{128}a_\vartheta - a_6\right)\left(\frac{\pi\mu}{\vartheta}\right)^{2/2} + O\left[\left(\frac{\pi\mu}{\vartheta}\right)^{3/2}\right] \tag{80}$$

where

$$a_2 = \frac{\vartheta}{\pi}\int_0^\infty 2\tau^2 \frac{\operatorname{sech}^2 \pi\tau}{\tanh \pi\tau \tanh \vartheta\tau}\, d\tau \tag{81}$$

$$a_4 = \frac{\vartheta}{\pi}\int_0^\infty \left(\frac{7}{4}\tau^2 - \frac{1}{2}\tau^4\right)\frac{\operatorname{sech}^2 \pi\tau}{\tanh \pi\tau \tanh \vartheta\tau}\, d\tau \tag{82}$$

$$a_6 = \frac{\vartheta}{\pi}\int_0^\infty \frac{1}{18}\left(\frac{439}{16}\tau^2 - \frac{55}{4}\tau^4 + \tau^6\right) \times \frac{\operatorname{sech}^2 \pi\tau}{\tanh \pi\tau \tanh \vartheta\tau}\, d\tau. \tag{83}$$

Substituting the estimates for $A_1^{(0)}$, $A_3^{(0)}$, $A_5^{(0)}$, and $A_7^{(0)}$ into (56) and rearranging, we obtain

$$\frac{\kappa}{Nu_S} = \frac{\mu}{2}\left(\frac{\pi\mu}{\vartheta}\right)^{-1/2} + \frac{\mu}{2}\left[-2a_\vartheta + C_1^{(4)}\kappa^{1/2} + \frac{1}{2}C_3^{(4)}\kappa^{3/2} + \frac{27}{32}C_5^{(4)}\kappa^{5/2} + \frac{125}{64}C_7^{(4)}\kappa^{7/2} + \cdots\right]$$

$$+\frac{\mu}{2}\left(\frac{\pi\mu}{\vartheta}\right)^{1/2}\left[\left\{\frac{1}{2}\left(\frac{\vartheta^2}{\pi^2}-1\right)+4a_\vartheta^2\right\}\right.$$
$$-2a_2C_3^{(4)}\kappa^{3/2}-\left(2a_4+\frac{9}{2}a_2\right)C_5^{(4)}\kappa^{5/2}$$
$$\left.-\left(2a_6+\frac{25}{2}a_4+\frac{225}{32}a_2\right)C_7^{(4)}\kappa^{7/2}-\cdots\right]$$
$$+\frac{\mu}{2}O\left(\frac{\pi\mu}{\vartheta}\right). \tag{84}$$

A leading-order estimate of a_ϑ is

$$a_\vartheta \sim \frac{1}{3\pi}\left(\frac{\vartheta^2}{\pi^2}-4\right) \tag{85}$$

which means that $C_1^{(4)}\kappa^{1/2}$ cannot be ignored in comparison with $-2a_\vartheta$, even at the relatively small value of $\kappa = 0.1$. Then, it is seen from (84) that for $k_l \ll k_s$, droplet thermal interactions start to take place after the leading order in $\mu^{1/2}$. Thus, for moderate conductivity ratios (i.e. $\mu \sim 0.01$), the interactions between the droplets through the solid can be quite important.

When $\mu \to 0$, droplet thermal interactions through the solid can be neglected because the effect is short-range in terms of the distance from the drops. However, the solid thermal conductivity must still be incorporated into the calculations of heat transfer. In this case, (84) reduces to

$$Q = 2\pi R\left(\frac{\pi}{\vartheta}\right)^{1/2}(k_l k_s)^{1/2}\Delta T. \tag{86}$$

For a fixed k_l, the rate of heat flow into a droplet becomes infinite as $\mu \to 0$. The reason is as follows: when $\mu \to 0$, the solid surface becomes isothermal, causing a temperature discontinuity at the edge of the droplet. As a result, the heat flux at the contact line becomes singular. This singularity is non-integrable, and leads to an infinite Q.

It has been shown rigorously [22] that a temperature jump at the edge of a droplet results in an infinite rate of heat flow through the droplet. Thus, to avoid an infinite heat transfer rate, the boundary condition of an isothermal solid surface should never be employed. Instead, the surface temperature must be allowed to vary so that at the contact line, it is equal to that of the liquid–vapor interface. Clearly, this can be achieved only with the incorporation of the solid into the analysis. In fact, the calculations performed by Sadhal and Plesset [2] for a *single* hemispherical droplet show that the temperature at the solid–liquid interface is non-uniform. In view of the fairly common practice of modeling dropwise evaporation with droplets on isothermal solid surfaces and excluding the solid material, these points are indeed worthy of consideration.

Table 1. Expression for the coefficients of the series expansions of $1/Nu$, $m = 4, 6$

n	$G_nA_1^{(0)}$
0	1
1	$C_1^{(m)}A_1^{(0)}$
3	$2A_3^{(0)}C_3^{(m)}$
5	$\left[2A_5^{(0)}+9\frac{A_3^{(0)}A_3^{(0)}}{A_1^{(0)}}\right]C_5^{(m)}$
6	$-[\frac{1}{4}A_1^{(0)}A_1^{(0)}-3A_1^{(0)}A_3^{(0)}+4A_1^{(0)}A_5^{(0)}-A_3^{(0)}A_3^{(0)}](C_3^{(m)})^2$
7	$\left[2A_7^{(0)}+50\frac{A_3^{(0)}A_5^{(0)}}{A_1^{(0)}}\right]C_7^{(m)}$

7.3. *Numerical results*

While (84) is valid for small μ such that $(\pi\mu/\vartheta)^{1/2} \ll 1$, the integrals in (30)–(33) must, in general, be evaluated numerically. Also, there is practical interest in knowing Nu, or the heat transfer coefficient, h, for that matter. We have summarized the numerical results in tabular forms. The Nusselt number ($Nu = hR/k_l$) can be expressed as

$$\frac{1}{Nu} = \frac{\mu}{2\kappa}\{G_0+G_1\kappa^{1/2}+G_3\kappa^{3/2}+G_5\kappa^{5/2}$$
$$+G_6\kappa^{6/2}+G_7\kappa^{7/2}+O(\kappa^{8/2})\} \tag{87}$$

where the coefficients G_n are given in Table 1. The numerical values of the array sums $C_n^{(m)}$ are given in Table 2. In Tables 3–6, the coefficients $A_1^{(0)}$, $A_3^{(0)}$, $A_5^{(0)}$, and $A_7^{(0)}$, respectively, are tabulated as functions of the conductivity ratio and droplet contact angle. For a given κ, the Nusselt number is then readily calculated using (87). However, since the expressions for the Nusselt number involve an infinite series, we first have to determine the appropriate number of terms needed to obtain accurate results. For $\kappa = 0.7$, which represents the case of nearly touching droplets arranged in a square array, $\pi/12 \leqslant \vartheta \leqslant \pi/2$, and $0.001 \leqslant \mu \leqslant 1$, the difference between using the first four terms and the first six terms of (87) is always less than 4.2%. Furthermore, this relatively large difference occurs only when $\mu \sim 1$. For water droplets evaporating on most metals, $\mu \sim 0.01$, and for $\mu = 0.01$,

Table 2. The array sums $C_n^{(m)}$

	$m = 4$ (square)	$m = 6$ (hexagon)
$C_1^{(m)}$	−2.20049	−2.21220
$C_3^{(m)}$	1.62232	1.59703
$C_5^{(m)}$	0.29098	0.26979
$C_7^{(m)}$	0.08048	0.06814

Table 3. The coefficient $A_1^{(0)}$ as a function of ϑ and μ

μ	$\vartheta = \pi/12$	$\vartheta = \pi/6$	$\vartheta = \pi/4$	$\vartheta = \pi/3$	$\vartheta = \pi/2$
0.001	0.09961	0.07243	0.05990	0.05228	0.04312
0.002	0.13554	0.09966	0.08284	0.07254	0.06007
0.004	0.18168	0.13564	0.11355	0.09987	0.08316
0.006	0.21371	0.16136	0.13580	0.11983	0.10021
0.008	0.23864	0.18185	0.15371	0.13602	0.11414
0.010	0.25916	0.19905	0.16889	0.14980	0.12609
0.020	0.32817	0.25949	0.22330	0.19985	0.17017
0.040	0.40104	0.32867	0.28800	0.26079	0.22546
0.060	0.44259	0.37136	0.32949	0.30080	0.26287
0.080	0.47048	0.40171	0.35983	0.33061	0.29139
0.100	0.49081	0.42487	0.38353	0.35424	0.31442
0.200	0.54473	0.49160	0.45498	0.42761	0.38872
0.400	0.58300	0.54545	0.51704	0.49457	0.46103
0.600	0.59862	0.56964	0.54661	0.52781	0.49897
0.800	0.60716	0.58356	0.56423	0.54812	0.52293
1.000	0.61256	0.59265	0.57600	0.56192	0.53960

Table 4. The coefficient $A_3^{(0)}$ as a function of ϑ and μ

μ	$\vartheta = \pi/12$	$\vartheta = \pi/6$	$\vartheta = \pi/4$	$\vartheta = \pi/3$	$\vartheta = \pi/2$
0.001	0.024068	0.017669	0.014673	0.012838	0.010614
0.002	0.032311	0.024073	0.020126	0.017682	0.014693
0.004	0.042517	0.032320	0.027271	0.024095	0.020162
0.006	0.049333	0.038057	0.032334	0.028690	0.024132
0.008	0.054475	0.042530	0.036339	0.032355	0.027333
0.010	0.058594	0.046213	0.039678	0.035435	0.030047
0.020	0.071635	0.058609	0.051232	0.046271	0.039791
0.040	0.083847	0.071643	0.064042	0.058677	0.051385
0.060	0.089962	0.078983	0.071660	0.066302	0.058801
0.080	0.093665	0.083833	0.076906	0.071688	0.064203
0.100	0.096139	0.087307	0.080796	0.075767	0.068400
0.200	0.101629	0.096071	0.091280	0.087234	0.080831
0.400	0.104391	0.101527	0.098601	0.095858	0.091093
0.600	0.105186	0.103398	0.101380	0.099363	0.095641
0.800	0.105526	0.104284	0.102783	0.101211	0.098183
1.000	0.105704	0.104781	0.103605	0.102329	0.099789

Table 5. The coefficient $A_5^{(0)}$ as a function of ϑ and μ

μ	$\vartheta = \pi/12$	$\vartheta = \pi/6$	$\vartheta = \pi/4$	$\vartheta = \pi/3$	$\vartheta = \pi/2$
0.001	0.0133078	0.0098175	0.0081700	0.0071570	0.0059254
0.002	0.0177421	0.0133092	0.0111601	0.0098215	0.0081768
0.004	0.0231240	0.0177441	0.0150346	0.0133156	0.0111717
0.006	0.0266402	0.0207845	0.0177476	0.0157929	0.0133270
0.008	0.0292447	0.0231257	0.0198723	0.0177528	0.0150526
0.010	0.0312967	0.0250330	0.0216289	0.0193871	0.0165064
0.020	0.0375494	0.0312935	0.0275867	0.0250396	0.0216524
0.040	0.0429275	0.0375345	0.0339223	0.0312844	0.0275993
0.060	0.0453420	0.0408320	0.0375114	0.0349694	0.0312796
0.080	0.0466607	0.0428904	0.0398806	0.0374825	0.0338862
0.100	0.0474546	0.0442880	0.0415696	0.0393249	0.0358601
0.200	0.0487874	0.0473797	0.0457143	0.0441239	0.0413680
0.400	0.0489411	0.0486960	0.0479860	0.0471185	0.0453283
0.600	0.0487808	0.0488799	0.0485575	0.0480360	0.0467839
0.800	0.0486319	0.0488558	0.0487205	0.0483877	0.0474614
1.000	0.0485142	0.0487848	0.0487497	0.0485298	0.0478155

Table 6. The coefficient $A_7^{(0)}$ as a function of ϑ and μ

μ	$\vartheta = \pi/12$	$\vartheta = \pi/6$	$\vartheta = \pi/4$	$\vartheta = \pi/3$	$\vartheta = \pi/2$
0.001	0.0091359	0.0067621	0.0056354	0.0049408	0.0040944
0.002	0.0121235	0.0091364	0.0076766	0.0067638	0.0056386
0.004	0.0156994	0.0121239	0.0103016	0.0091387	0.0076815
0.006	0.0179993	0.0141511	0.0121247	0.0108108	0.0091433
0.008	0.0196803	0.0156988	0.0135428	0.0121260	0.0103081
0.010	0.0209886	0.0169499	0.0147082	0.0132171	0.0112852
0.020	0.0248597	0.0209825	0.0186051	0.0169455	0.0147104
0.040	0.0279618	0.0248431	0.0226241	0.0209605	0.0185882
0.060	0.0292146	0.0267790	0.0248167	0.0232581	0.0209313
0.080	0.0298203	0.0279275	0.0262146	0.0247822	0.0225561
0.100	0.0301331	0.0286675	0.0271776	0.0258703	0.0237625
0.200	0.0303797	0.0300721	0.0293349	0.0285174	0.0269670
0.400	0.0299727	0.0303098	0.0301829	0.0298536	0.0289834
0.600	0.0296480	0.0301159	0.0302020	0.0300828	0.0295601
0.800	0.0294281	0.0299105	0.0300824	0.0300667	0.0297401
1.000	0.0292730	0.0297372	0.0299447	0.0299841	0.0297770

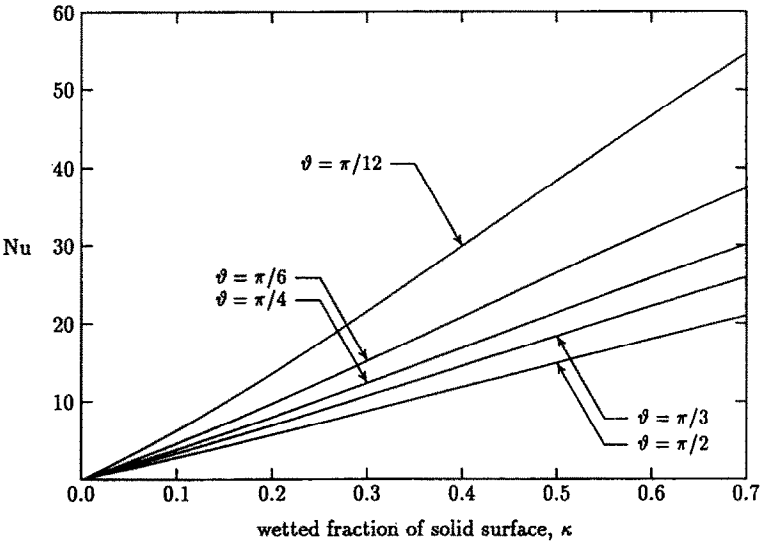

FIG. 5. Nusselt number Nu for a square array of droplets. The conductivity ratio is $\mu = 0.01$.

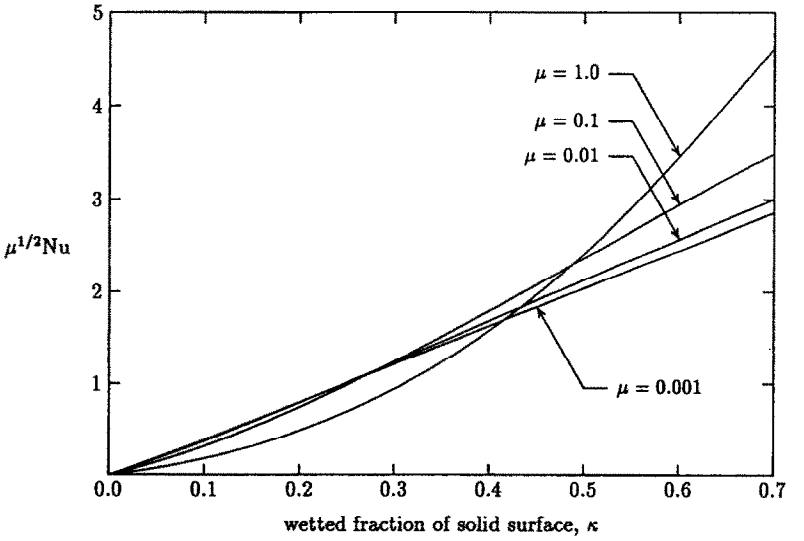

FIG. 6. Nusselt number Nu for a square array of droplets with a contact angle of $\vartheta = \pi/4$.

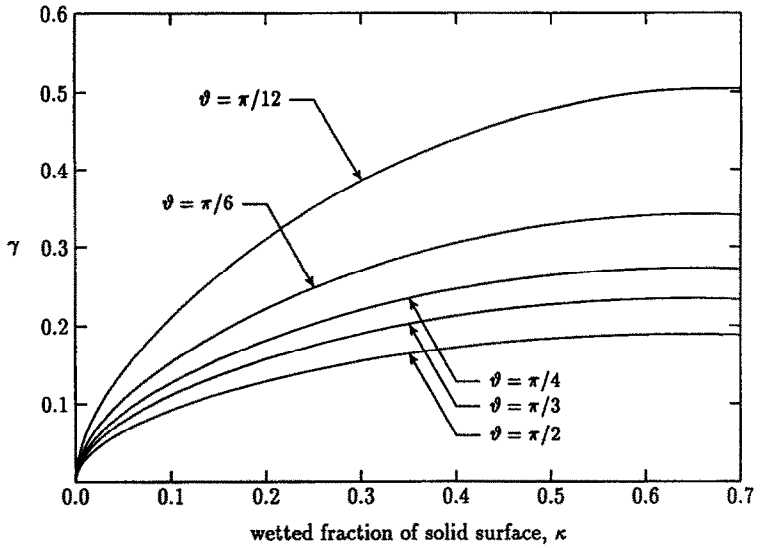

FIG. 7. Deviation from $Nu_{\kappa=0}$, γ, of a square array of droplets. The conductivity ratio is $\mu = 0.01$.

the difference never exceeds 1.4%. Thus, for practical purposes (with the restriction of $\pi/12 \leqslant \vartheta \leqslant \pi/2$), equation (87), in which the actual errors may be smaller than the figures cited above, is adequate.

Figures 5 and 6 show the dependence of the Nusselt number on κ, μ, and ϑ for a square array of droplets. It is seen that Nu decreases when ϑ or μ increase (note that Fig. 6 is a plot of $\mu^{1/2}Nu$ vs κ). Furthermore, the Nu–κ relationship is almost linear for small values of μ and large contact angles, thus qualitatively confirming (84). More generally, inspection of (87) reveals that the dependence of Nu on κ consists of a leading term proportional to κ and higher-order interaction terms. This leading term simply states that the average surface heat flux increases as the number of droplets (of a fixed size) on the solid surface increases. This heat flux is, however, augmented by the higher-order interaction terms, which may become significant for large values of κ, yielding the actual $\bar{q}$. Thus, the quantity γ, where

$$\gamma \equiv \frac{Nu - Nu_{\kappa=0}}{Nu_{\kappa=0}}, \tag{88}$$

can be regarded as a measure of the strength of droplet thermal interactions. In (88), $Nu_{\kappa=0}$ is given by

$$Nu_{\kappa=0} = \frac{2A_1^{(0)}}{\mu}\kappa \tag{89}$$

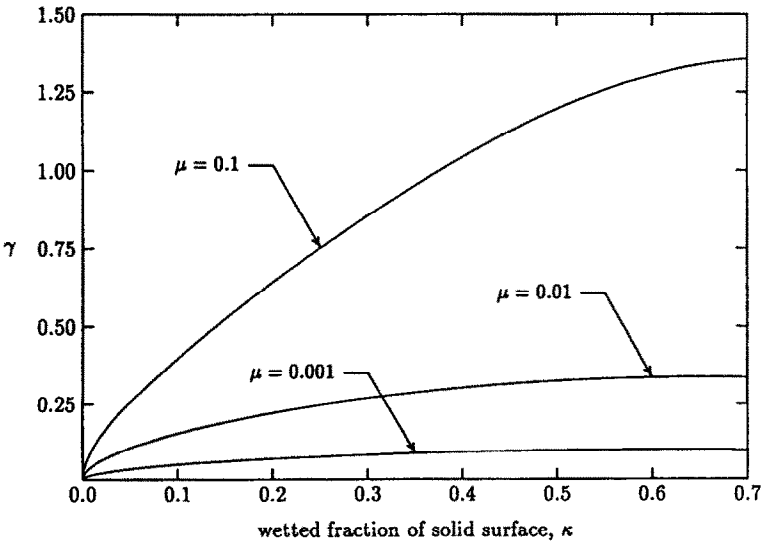

FIG. 8. Deviation from $Nu_{\kappa=0}$, γ, of a square array of droplets with a contact angle of $\vartheta = \pi/6$.

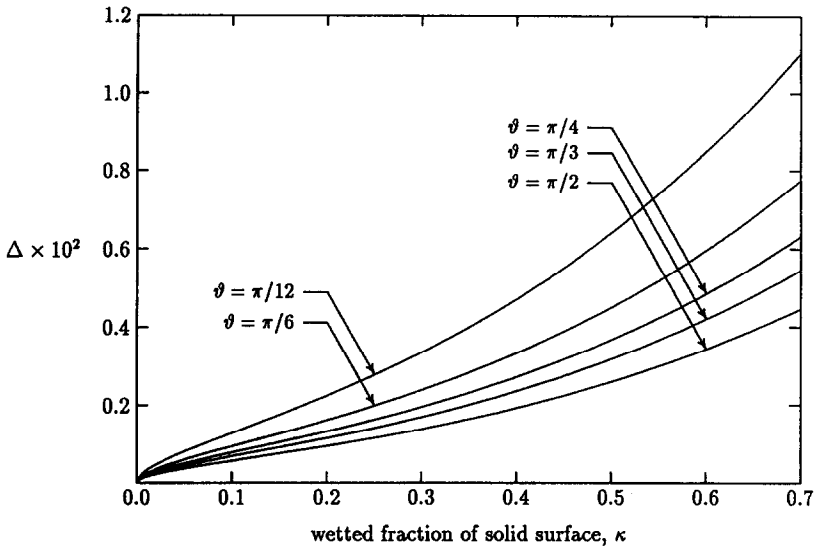

FIG. 9. Relative difference in Nusselt number, Δ, between a hexagonal and a square array of droplets with a conductivity ratio of $\mu = 0.01$.

which is the result obtained by neglecting droplet interactions. As expected, γ increases with κ (Figs. 7 and 8). Furthermore, for a fixed κ, γ decreases when μ decreases but increases with decreasing ϑ. Thus, droplet thermal interactions become stronger as the contact angle or solid conductivity decreases. From Fig. 8, we can infer that droplet interactions are negligible for the entire range of $0 \leqslant \kappa \leqslant 0.7$ when $\mu \to 0$. This is in accordance with the asymptotic analysis of $(\pi\mu/\vartheta)^{1/2} \to 0$ carried out earlier. However, for the commonly encountered cases of $\mu \sim 0.01$, the interactions are quite significant, even at moderate values of κ (see Fig. 7). In Figs. 9 and 10, we plot the relative difference in Nu between a square array and a hexagonal array of droplets,

$$\Delta \equiv \frac{Nu_{\mathrm{H}} - Nu_{\mathrm{S}}}{Nu_{\mathrm{S}}}, \tag{90}$$

as a function of κ, ϑ and μ being the parameters. As expected, the effect of κ, ϑ, and μ on Δ is qualitatively similar to that on γ. This is so because Δ is a function of the strength of droplet interactions. When $\gamma \ll 1$, the effect of droplet spatial arrangement on the Nusselt number is negligible. On the other hand, Δ may

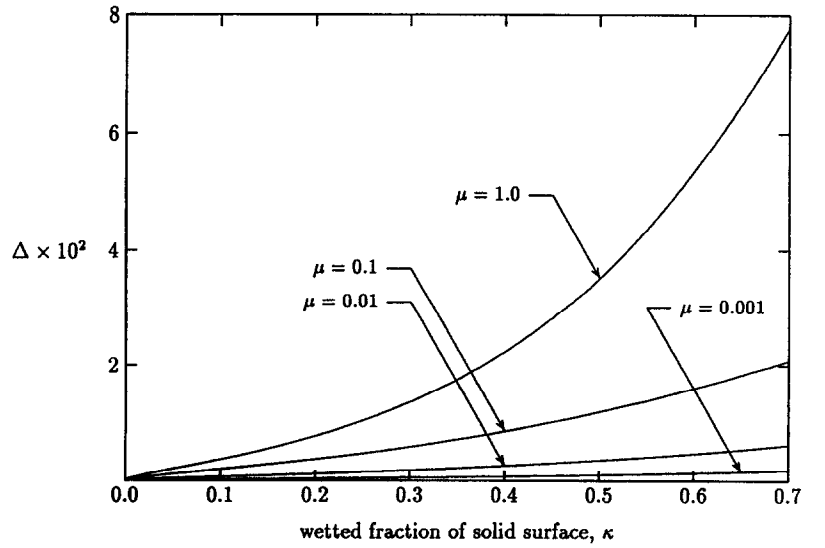

FIG. 10. Relative difference in Nusselt number, Δ, between a hexagonal and a square array of droplets with a contact angle of $\vartheta = \pi/4$.

become significant when droplet interactions become stronger. From Figs. 9 and 10, we can conclude that a hexagonal array and a square array of droplets with $\pi/12 \leqslant \vartheta \leqslant \pi/2$ and $\mu \sim 0.01$ or smaller yield a practically identical Nusselt number.

8. CONCLUSION

This work represents a first theoretical attempt to deal with the problem of a large number of droplets evaporating from a heated surface. While we have obtained expressions for the Nusselt number, the major challenge of dealing with a spatially random distribution of droplets with a spectrum of sizes, which will be encountered in the analyses involving droplet sprays, still remains. Further effort for both low and intermediate superheat regimes is presently needed to develop proper practical models. The statistical approach to this class of problems is currently under examination.

Acknowledgements—The research reported here was conducted by the authors while the first (K.-K. Tio) was a Ph.D. student in the Department of Mechanical Engineering at the University of Southern California. Financial support from the U.S. National Science Foundation (Grant Nos. CBT-8351432 and INT-8807482) is gratefully acknowledged. Thanks are also due to D.A.M.T.P. (Cambridge University) for the availability of their research facilities to the second author (S. S. Sadhal), who was on a sabbatical leave there (1 July 1988–18 July 1989).

REFERENCES

1. W.-J. Yang, Mechanics of droplet evaporation on heated surfaces, *Lett. Heat Mass Transfer* **5,** 151–166 (1978).
2. S. S. Sadhal and M. S. Plesset, Effect of solid properties and contact angle in dropwise condensation and evaporation, *J. Heat Transfer* **101,** 48–54 (1979).
3. C. Bonacina, S. Del Giudice and G. Comini, Dropwise evaporation, *J. Heat Transfer* **101,** 441–446 (1979).
4. W. M. Grissom and F. A. Wierum, Liquid spray cooling of a heated surface, *Int. J. Heat Mass Transfer* **24,** 261–271 (1981).
5. J. J. Rizza, A numerical solution to dropwise evaporation, *J. Heat Transfer* **103,** 501–507 (1981).
6. N. Zhang and W.-J. Yang, Micro-structure of flow inside minute drops evaporating on a surface, *J. Heat Transfer* **105,** 908–910 (1983).
7. N. Zhang and W.-J. Yang, Evaporation and explosion of liquid drops on a heated surface, *Exp. Fluids* **1,** 101–111 (1983).
8. A. K. Sen and C. K. Law, On a slowly evaporating droplet near a hot plate, *Int. J. Heat Mass Transfer* **27,** 1418–1421 (1984).
9. C. T. Avedisian and J. Koplik, Leidenfrost boiling of methanol droplets on hot porous/ceramic surfaces, *Int. J. Heat Mass Transfer* **30,** 379–393 (1987).
10. T. K. Nguyen and C. T. Avedisian, Numerical solution for film evaporation of a spherical liquid droplet on an isothermal and adiabatic surface, *Int. J. Heat Mass Transfer* **30,** 1497–1509 (1987).
11. S. Zhang and G. Gogos, Film evaporation of a spherical droplet over a hot surface: fluid mechanics and heat/mass transfer analysis, *J. Fluid Mech.* **222,** 543–563 (1991).
12. K.-K. Tio, Transport problems with spatially periodic mixed interface conditions, Ph.D. Thesis, University of Southern California, Los Angeles (1990).
13. N. N. Lebedev, *Special Functions and their Applications.* Dover, New York (1972).
14. I. N. Sneddon, *The Use of Integral Transforms.* McGraw-Hill, New York (1972).
15. M. S. Plesset, Note on the flow of vapor between liquid surfaces, *J. Chem. Phys.* **20,** 790–793 (1952).
16. S. S. Sadhal, Comments about Yang's analysis on droplets evaporating from a solid surface, *Lett. Heat Mass Transfer* **6,** 149–155 (1979).
17. J. C. Han and W.-J. Yang, Thermal instability in liquid droplets on a heated surface, *J. Heat Transfer* **102,** 581–583 (1980).
18. N. Zhang, Z. Jiang and W.-J. Yang, Thermal stability in evaporating liquid disks by local potential technique, *J. Thermophys. Heat Transfer* **3,** 195–202 (1989).
19. J. R. A. Pearson, On convection cells induced by surface tension, *J. Fluid Mech.* **4,** 489–500 (1958).
20. D. A. Nield, Surface tension and buoyancy effects in cellular convection, *J. Fluid Mech.* **19,** 341–352 (1964).
21. J. J. Lorenz and B. B. Mikic, The effect of thermocapillary flow on heat transfer in dropwise condensation, *J. Heat Transfer* **92,** 46–52 (1970).
22. S. S. Sadhal and W. W. Martin, Heat transfer through drop condensate using differential inequalities, *Int. J. Heat Mass Transfer* **20,** 1401–1407 (1977).

EVAPORATION DE GOUTTES: ANALYSE THERMIQUE DES SYSTEMES MULTIGOUTTES

Résumé—On étudie le transfert de chaleur d'une surface chaude solide vers des guottelettes qui s'évaporent dans un régime de faible surchauffe, les gouttelettes restant collées à la surface sans nucléation. Le modèle concerne un arrangement régulier de gouttelettes identiques étant en interaction thermique avec le solide. On obtient des expressions analytiques pour le nombre de Nusselt impliquant une série puissance de $\kappa^{1/2}$, ou κ est la fraction de surface solide mouillée par les gouttelettes. On trouve que les interactions de gouttelettes ne peuvent pas être ignorées en général. La force de ces interactions est fonction de l'angle de contact de la gouttelette, de la conductivité du solide et de la concentration en gouttes.

TROPFENVERDAMPFUNG: THERMISCHE UNTERSUCHUNG EINES SYSTEMS AUS VIELEN TROPFEN

Zusammenfassung—In der vorliegenden Arbeit wird der Wärmeübergang von einer beheizten festen Oberfläche an Tröpfchen, die im Bereich der kleinen Überhitzung verdampfen, untersucht. Dabei haften die Tröpfchen an der Oberfläche, ohne daß sich Blasen bilden. Das Modell besteht aus einer regelmäßigen Anordnung von gleichen Tröpfchen, die über die feste Oberfläche in thermischer Wechselwirkung miteinander stehen. Analytische Ausdrücke für die Nusselt-Zahl, die den Faktor $\kappa^{1/2}$ enthalten, werden hergeleitet. Dabei ist κ der mit Tröpfchen benetzte Anteil der festen Oberfläche. Es wird festgestellt, daß die Wechselwirkungen zwischen den Tröpfchen nicht immer vernachlässigt werden können. Vielmehr ist die Stärke dieser Wechselwirkungen eine Funktion des Randwinkels der Tröpfchen, der Wärmeleitfähigkeit des Festkörpers und der Konzentration der Tröpfchen.

КАПЕЛЬНОЕ ИСПАРЕНИЕ: ТЕРМИЧЕСКИЙ АНАЛИЗ МНОГОКАПЕЛЬНЫХ СИСТЕМ

Аннотация—Исследуется теплоперенос от нагретой поверхности твердого тела к каплям, испаряющимся в режиме малого перегрева, в случае прилипания капель к поверхности при отсутствии пузырькового зародышеобразования. Модель предполагает правильное расположение одинаковых капель, термически взаимодействующих посредством теплообмена с твердым телом. Выводятся аналитические выражения для числа Нуссельта, включающие степенной ряд по $\kappa^{1/2}$, где κ-доля поверхности твердого тела, смачиваемая каплями. Найдено, что, в общем, взаимодействиями капель нельзя пренебрегать. При этом сила цказанных взаимодействий зависит от угла контакта капель, теплопроводности твердого тела и концентрации капель.